Dalton Transactions

Accepted Manuscript

ROYAL SOCIETY OF CHEMISTRY

www.rsc.org/dalton

Four tetrazolate-based 3D frameworks with diverse subunits directed by inorganic anions and azido coligand: Hydro/solvothermal syntheses, crystal structures, and magnetic properties

Zhao-Jun Hou,[a] Zhong-Yi Liu,[a] Ning Liu,[a] En-Cui Yang[a,*] and Xiao-Jun Zhao[a,b,*]

To *Dalton Trans* (Article)

[a] *College of Chemistry, Key Laboratory of Inorganic-Organic Hybrid Functional Material Chemistry, Ministry of Education, Tianjin Key Laboratory of Structure and Performance for Functional Molecules, Tianjin Normal University, Tianjin 300387, P. R. China. E-mail: encui_yang@163.com, xiaojun_zhao15@163.com; Fax:+86-22-23766556*

[b] *Collaborative Innovation Center of Chemical Science and Engineering (Tianjin), Tianjin 300071, P. R. China*

† Electronic supplementary information (ESI) available: Additional figures for **1** and **2**, PXRD patterns, and X-ray crystallographic files in CIF format for **1**–**4**. CCDC 1018186–1018189 for **1**–**4**. For ESI and crystallographic data in CIF or other electronic format see DOI:10.1039/

Four tetrazolate (tz^-)-based magnetic metal-organic frameworks, $[Cu_5(\mu_3\text{-}OH)_2(SO_4)_2(tz)_4]_n$ (**1**), $\{[Cu_3(tz)_4Cl_2]\cdot 1.4CH_3OH\}_n$ (**2**), $[Cu(N_3)(tz)]_n$ (**3**) and $\{[Cu_5(tz)_9]Cl\cdot 4H_2O\}_n$ (**4**), were hydro/solvothermally synthesized, and structurally and magnetically characterized. Structural analyses reveal that the former two samples are the same eight-connected topological frameworks assembled from different subunits. Hourglass-shaped $\{Cu_5(\mu_3\text{-}OH)_2\}^{8+}$ cores in **1** are periodically extended by mixed μ_3-/μ_4-tz^- and μ_4-SO_4^{2-} heterolinkers. While the linear $\{Cu_3(\mu\text{-}Cl)_2\}^{4+}$ blocks in **2** are repeatedly intersected by ditopic μ_3-tz^- connectors. By contrast, square grid-shaped network of **3** is constructed from linear $\{Cu(\mu_{1,1}\text{-}N_3)\}^+$ chain and μ_3-tz^- linkers. Complex **4** consists of trigonal-prismatic $\{Cu_8(\mu_3\text{-}tz)_6\}^{10+}$ subunits, which are interlinked into hexagonal microporous architecture by mirror-symmetry μ_4-tz^- ligands. Thus, the various subunits of **1–4** are significantly tuned by the co-coordination of the inorganic anions and/or the azido coligand, and the backbone extensions are directed by the polytopic tetrazolate ligand. Magnetically, different ordering arrangements of the non-zero magnetizations produced in the local Cu^{II}_5 and Cu^{II}_3 subunits lead eventually to unusual ferrimagnet and canted antiferromagnet for **1** and **2**. Strong antiferromagnetic couplings mediated by the mixed tz^- and/or azido bridges result in overall $S = 0$ spin ground-states of **3** and **4**.

Introduction

Magnetic metal-organic frameworks (MMOFs) are of great interest and essential importance due to their aesthetically pleasing structures as well as potentially fascinating applications in quantum computation and high-density information storage.[1] Synthetically speaking, single or mixed short magnetic bridges, such as linear azido,[2–4] bent carboxylate,[5–7] cyclic polyzolate and so on,[8–12] have been widely used and gradually becoming excellent candidates for the targeted MMOFs. Especially, modified by four sequent electron-donating N-donors, 1H-tetrazole (Htz) and its abundant derivatives have generated numerous MOFs with intriguing topologies and interesting magnetic, absorptive and photophysical properties, which are vitally resulting from their diverse coordination modes, asymmetric magnetic superexchange, as well as inert and hydrophobic pore surface.[13–16] Moreover, substitute effects during self-assembly processes have also been explored by appending different groups (substituent, pendant or side groups) to the coplanar five-membered azolyl ring.[11, 17] However, to the best of our knowledge, only limited entities with unsubstituted tetrazolate ligand have been reported by far,[18–21] which thus provides good opportunities to continue the magnetostructural investigations of the tetrazolate-based MMOFs.

Small inorganic anions, such as Cl^-, SO_4^{2-}, ClO_4^-, NO_3^- and so on, can serve either as counteranions to assist the generation of the crystalline products[22–23] or as co-coordinating groups to take part in the direct binding towards the metal ions contributing for novel and unexpected inner-sphere metal complexes.[24–28] Crystallographically, the co-coordination of the inorganic anion can significantly tune the structural subunits and even the overall skeletal diversities.[29–31] Magnetically, due to the different superexchange couplings, some intriguing samples with unusual $\mu_{1,3}$- and $\mu_{1,1}$-nitrito/nitrato bridges have exhibited moderate antiferromagnetic and ferromagnetic behavior.[32–33] Photophysically, selective fluorescence sensing for small molecules and volatile gases,[24–25] anion-responsive photoluminescence and anion

separation[31] have also been achieved by chloride and bromide-participated metal complexes, which can be considered as a useful method to monitor the anion-exchange process. Unfortunately, it is still challenging and currently difficult to exactly control the role of small inorganic anion during the self-assembly process. Herein, in the present work, sterically unencumbered 1-H-tetrazole (Htz) was chosen as effective magnetic mediator to react with different inorganic Cu(II) slats under controllable hydro/solvothermal conditions in the absence and presence of azido anion. The particular purpose of the investigation focused on the influences of the inorganic anions/azido coligand on the structure and magnetic behavior and the understanding of the inherent magnetostructural relationships. As a result, four new three-dimensional (3D) frameworks with hourglass-shaped $\{Cu_5(\mu_3\text{-}OH)_2\}^{8+}$ cluster, linear $\{Cu_3(\mu\text{-}Cl)_2\}^{4+}$ core, linear $\{Cu(\mu_{1,1}\text{-}N_3)\}^{+}$ chain, and trigonal-prismatic $\{Cu_4(\mu_3\text{-}tz)_3\}^{5+}$ subunit were successfully fabricated and fully characterized structurally and magnetically. Crystallographically, the co-coordination of the inorganic anions/azido coligand with tz^- block significantly directs the structural subunits of the targeted frameworks by their different coordination abilities, bridging modes and steric hindrance. Magnetically, on the other hand, different alignments of the non-zero net magnetic moments produced in the antiferromagnetically coupled Cu^{II}_5 and Cu^{II}_3 subunits lead to ferrimagnet and canted antiferromagnet. Strong and comparable antiferromagnetic couplings mediated by the mixed heterobridges result in the overall $S = 0$ spin ground-states of the latter two complexes.

Experimental section

Materials and instruments

All initial chemicals were commercially purchased (1-H-teatrazole were from TCI (shanghai) Development Co., Ltd. and other analytical-grade reagents were from Tianjin Chemical Reagent Factory) and used as received without further purification. Elemental analyses for C, H and N were carried out with a CE-440

(Leeman-Labs) analyzer. Fourier transform (FT) IR spectra (KBr pellets) were taken on an Avatar-370 (Nicolet) spectrometer in the range 4000–400 cm^{-1}. Powder X-ray diffraction (PXRD) patterns were obtained from a Bruker D8 ADVANCE diffractometer at 40 kV and 40 mA for Mo *K*α radiation (λ = 1.5406 Å), with a scan speed of 0.1 sec/step and a step size of 0.01° in 2*θ*. The simulated PXRD pattern was calculated using single-crystal X-ray diffraction data and processed by the free *Mercury v1.4* program downloaded from the Cambridge Crystallographic Data Center. Magnetic susceptibilities were acquired on a Quantum Design (SQUID) magnetometer MPMS-XL-7 with polycrystalline samples, in which the phase purity of the bulk samples was determined by PXRD experiments. The diamagnetic corrections were calculated using Pascal's constants, and an experimental correction for the sample holder was also applied.

Synthesis of 1–4

$[Cu_5(\mu_3\text{-}OH)_2(SO_4)_2(tz)_4]_n$ (1). A mixture containing Htz (14.0 mg, 0.2 mmol) and $CuSO_4·5H_2O$ (74.9 mg, 0.3 mmol) was dissolved in mixed mehanol-water solution (v:v = 7:3, 10.0 mL). The initial pH value of the mixture was adjusted to ca. 6 by aqueous NaOH solution (0.25 M). The resulting mixture was then transferred into a parr Teflon-lined stainless steel vessel (23.0 mL) and heated at 140 °C for 72 h under autogenous pressure. After the mixture was cooled to room temperature at a rate of 2.5 $°C·h^{-1}$, blue block-shaped crystals suitable for X-ray analysis were obtained directly, washed with methanol, and dried in air (Yield: 35% based on Htz). Anal. Calcd for $C_8H_{12}Cu_{10}N_{32}O_{20}S_4$: C 5.86, H 0.74, N 27.33%. Found: C 5.85, H 0.73, N 27.35%. IR (KBr, cm^{-1}): 3573(w), 3357(w), 3136(w), 1473(m), 1277(m), 1233(m), 1179 (m), 1138(s), 1061(w), 1014(m), 997(m), 875(m), 685(w), 641(w), 599(w), 457(w).

$\{[Cu_3(tz)_4Cl_2]·1.4CH_3OH\}_n$ (2). A mixture containing Htz (14.0 mg, 0.2 mmol) and $CuCl_2·2H_2O$ (34.0 mg, 0.2 mmol) was dissolved in mixed methanol-water solution (v:v = 4:1, 10.0 mL), and the initial pH value of the mixture was adjusted to ca. 6 by aqueous NaOH solution (0.25 M). The resulting mixture was

then transferred into a parr Teflon-lined stainless steel vessel (23.0 mL) and heated at 130 °C for 72 h under autogenous pressure. After the mixture was cooled to room temperature at a rate of 2.3 °C·h^{-1}, blue block-shaped crystals suitable for X-ray analysis were obtained directly, washed with methanol, and dried in air (Yield: 40% based on Htz). Anal. Calcd for $C_{5.40}H_{9.60}Cl_2Cu_3N_{16}O_{1.40}$: C 11.13, H 1.66, N 38.47%. Found: C 10.06, H 1.68, N 38.25%. IR (KBr, cm^{-1}): 3405(br), 3098(w), 1451(m), 1331(m), 1267(m), 1122(s), 1030(s), 926(m), 694(w).

$[Cu(N_3)(tz)]_n$ (3). A mixture containing Htz (14.0 mg, 0.2 mmol), NaN_3 (26.0 mg, 0.4 mmol), $CuSO_4·5H_2O$ (74.9 mg, 0.3 mmol) and doubly deionized water (10.0 mL) was sealed in a parr Teflon-lined stainless steel vessel (23.0 mL) and heated at 130 °C for 96 h under autogenous pressure. After the mixture was cooled to room temperature at a rate of 2.3 °C·h^{-1}, blue block-shaped crystals suitable for X-ray analysis were obtained directly, washed with methanol, and dried in air (Yield: 33% based on Htz). Anal. Calcd for $CHCuN_7$: C 6.88, H 0.58, N 56.15%. Found: C 6.78, H 0.59, N 56.17%. IR (KBr, cm^{-1}): 2084(s), 1448(m), 1271(m), 1249(m), 1144(m), 1119(m), 1055(m), 1024(m), 869(w), 682(w), 574(w), 410(w).

Caution: *Azido salt of transition-metal complex is potentially explosive. Only a small amount of material should be prepared and handled with caution.*

$\{[Cu_5(tz)_9]Cl·4H_2O\}_n$ (4). A mixture containing Htz (21.0 mg, 0.3 mmol) and $CuCl_2·2H_2O$ (34.0 mg, 0.2 mmol) was dissolved in doubly deionized water (10.0 mL). The initial pH value of the mixture was adjusted to ca. 6.0 by aqueous NaOH solution (0.25 M). The resulting mixture was then transferred into a parr Teflon-lined stainless steel vessel (23.0 mL) and heated at 150 °C for 72 h under autogenous pressure. After the mixture was cooled to room temperature at a rate of 2.5 °C·h^{-1}, blue block-shaped crystals suitable for X-ray analysis were obtained directly, washed with methanol, and dried in air (Yield: 30% based on Htz). Anal. Calcd for $C_3H_{5.67}Cl_{0.33}Cu_{1.67}N_{12}O_{1.33}$: C 10.33, H 1.64, N 48.17%. Found: C 10.18, H

1.57, N 48.06%. IR (KBr, cm^{-1}): 3398(br), 3120(w), 2961(m), 2860(m), 1654(m), 1448(s), 1325(m), 1239(s), 1137(s), 1157(s), 1061(m), 1024(m), 888(w), 688(w), 495(w).

X-Ray data collection and structure determination

Diffraction intensities for **1–4** were collected on a Bruker APEX–II QUAZAR diffractometer equipped with graphite-monochromated Mo *K*α radiation with a radiation wavelength of 0.71073 Å by using the *φ*–*ω* scan technique. There was no evidence of crystal decay during data collection. Semiempirical multiscan absorption corrections were applied by SADABS,[34] and the program SAINT was used for integration of the diffraction profiles.[35] The structures were solved by direct methods and refined with the full-matrix least-squares technique using the SHELXS-97 and SHELXL-97 programs.[36] Anisotropic thermal parameters were assigned to all non-H atoms. The organic hydrogen atoms were generated geometrically. The H atoms attached to the water molecule were located from difference maps and refined with isotropic temperature factors. Lattice methanol molecule in **2** was positionally disordered between two positions with the same site occupancy of 0.35. Free chloride (Cl1 and Cl1′) and water molecule (O1 and O1′ as well as O2 and O2′) in the asymmetric unit of **4** were positionally disordered with the site occupancies of 0.0145 and 0.1521 to Cl1 and Cl1′, 0.107 and 0.060 to O1 and O1′, 0.417 and 0. 083 to O2 and O2′. The crystallographic data were given in Table 1.

/insert Table 1/

Results and discussion

Syntheses, FT-IR spectra and PXRD results

Crystalline products of **1**–**4** were directly isolated by solvo/hydrothermal reactions of inorganic Cu^{II} salt and Htz ligand in the absence or presence of azido anion. The molar ratio of the reactants (Cu^{II}/tz^{-} = 1.5:1 vs 1:1), reaction temperature (130–150°C) and medium (mehanol-water vs water) were essentially

important for the preparations of **1**–**4**, in which the latter two factors tuned the selective syntheses of **2** and **4** with/without the co-coordinated chloride ligand.

In the IR spectra, broad bands centered around 3400 cm^{-1} in **1**, **2** and **4** are assigned to the stretching vibrations of O–H, indicating the presence of free water molecule and/or hydroxyl group. Characteristic bands emerged at 1400–1500 cm^{-1} are coming from the stretching vibrations of the tetrazolyl group in **1**–**4**.[37] The weak band at 1179 cm^{-1} is assigned to the characteristic vibrations for the SO_4^{2-} group of **1**.[37] The strong absorption at 2084 cm^{-1} for **2** is resulting from the asymmetric stretching of N_3^- anion.[37] The phase purity and structural consistency of the bulk samples of **1–4** have also been evidenced by the comparisons of the experimental and computer-simulated PXRD patterns (Fig. S1 in the ESI).

Crystal structures of 1–4

$[Cu_5(\mu_3\text{-}OH)_2(SO_4)_2(tz)_4]_n$ (1). Complex **1** crystallizes in the monoclinic $P2_1/n$ space group, exhibiting an eight-connected topological framework with hourglass-like $\{Cu_5(\mu_3\text{-}OH)_2\}^{8+}$ cores periodically extended by mixed μ_4-SO_4^{2-}, μ_3- and μ_4-tz^- linkers. The asymmetric unit of **1** consists of two and a half Cu^{II} ions, two tz^- anions in μ_3- and μ_4-binding modes, one μ_3-OH^- group and one μ_4-SO_4^{2-} anion. Located at an inversion center, the Cu1 atom in **1** is surrounded by two axial O atoms from two symmetry-related SO_4^{2-} anions and four equatorial N_2O_2 donors belonging to two tz^- and two μ_3-OH^- groups (Fig. 1a), exhibiting an elongated octahedron with the axial Cu–O bond lengths moderate longer (0.3 Å) than those in the equatorial plane (Table S1 in the ESI). Lying at a general position, the distorted Cu2 octahedron is in an N_4O_2 donor set fulfilled by four different tz^- ligands, one SO_4^{2-} and one μ_3-OH^- group. By contrast, the Cu3 site is in a square-pyramidal O_3N_2 coordination environment with Addison parameter τ = 0.17. The Addison parameter is defined as an index of trigonality ($\tau = 1$) and square-pyramid ($\tau = 0$).[38] The basal plane of Cu3 ion is well defined by N_2O_2 atoms from two symmetry-related tz^- anions, one μ_3-OH^- group and one SO_4^{2-}

anion, and the sulfonate O atom is in the apical position with the axial Cu–O distance almost 0.3 Å longer than those in the basal plane (Table S1).

/insert Fig. 1/

The central Cu1 ion links two pairs of centrosymmetric Cu2 and Cu2A as well as Cu3 and Cu3A ions by two asymmetric μ_3-OH^- groups, generating a hourglass-like $\{Cu_5(\mu_3\text{-}OH)_2\}^{8+}$ core (Fig. 1a). The intermetallic distance separated by the μ_3-OH^- group is 3.4352(1), 3.4011(2) and 3.3371(2) Å for Cu1···Cu2, Cu1···Cu3 and Cu2···Cu3, which is one of important parameters for the intracore magnetic couplings. Each $\{Cu_5(\mu_3\text{-}OH)_2\}^{8+}$ core in **1** connects repeatedly with four adjacent neighbors in crystallographic a*b* plane by two pairs of tetrahedral μ_4-SO_4^{2-} groups and four μ_4-N1,N2,N3,N4-tz^- ligands with the nearest intercluster Cu3···Cu3 and Cu2···Cu2 separation of 3.2386(1) and 4.3261(2) Å (Fig. 1b). Simultaneously, four crystallographically equivalent μ_3-N1,N2,N4-tz^- anions can also aggregate one central $\{Cu_5(\mu_3\text{-}OH)_2\}^{8+}$ core and four neighbors in *bc* plane with the closet intercluster Cu2···Cu3 separation of 5.9447(2) Å (Fig. 1b). Thus, an new 3D framework of **1** is generated from the cationic $\{Cu_5(\mu_3\text{-}OH)_2\}^{8+}$ core, μ_4-SO_4^{2-}, μ_4-N1,N2,N3,N4- and μ_3-N1,N2,N4-tz^- connectors (Fig. 1c). Topologically, each $\{Cu_5(\mu_3\text{-}OH)_2\}^{8+}$ core in **1** is periodically surrounded by eight adjacent ones through four μ_3-N1,N2,N3-tz^-, four μ_4-N1,N2,N3,N4-tz^- and two μ_4-SO_4^{2-} anions, and can be considered as an 8-connected node. Instead, the μ_4-SO_4^{2-}, μ_3- and μ_4-tz^- ligands in **1** serve as three different kinds of ditopic connectors, because they all connect two adjacent Cu^{II}_5 clusters together. Consequently, **1** belongs to an eight-connected topology net with Schläfli symbol of $\{3^6\cdot4^{18}\cdot5^3\cdot6\}$ (Fig. 1c).

$\{[Cu_3(tz)_4Cl_2]\cdot1.4CH_3OH\}_n$ (2). Complex **2** crystallizes from the orthorhombic *Pnnm* space group, also displaying an eight-connected topological net with centrosymmetrically linear $\{Cu_3(\mu\text{-}Cl)_2\}^{4+}$ clusters periodically extended by anionic μ_3-N1,N2,N4-tz^- connectors. Each asymmetric unit of **2** contains

one-and-a-half Cu^{II} ions, two tz^- ligands with the same binding fashion, one bridging μ-Cl^- anion and disordered lattice methanol molecules. Locating at an inversion center, the Cu1 ion is hexa-coordinated by two axial Cl^- and four equatorial N atoms from four crystallographically equivalent tz^- anions, building axially elongated octahedral coordination surrounding (Fig. 2a). By contrast, Cu2 resides in a perfect square-pyramidal geometry defined by four basal N donors from four separate tz^- ligands and one apical Cl^- anion. Due to strong Jahn-Teller effect, the axial/apical Cu–Cl separations are much longer by 0.6–0.4 Å than those in the equatorial/basal planes (Table S2). The sole tz^- anion in **2** adopts an asymmetric μ_3-N1,N2,N4-binding mode to hold two Cu2 and one Cu1 ions together.

/insert Fig. 2/

The central Cu1 site aggregates two centrosymmetric Cu2 and Cu2C ions by a pair of μ-Cl^- anions, resulting in a linear $\{Cu_3(\mu\text{-}Cl)_2\}^{4+}$ subunit with the intermetallic separation of 3.4782(1) Å (Fig. 2a). The tz^- anion in **2** displays a μ_3-N1,N2,N4-binding mode to reinforce the adjacent Cu^{II} ions within the linear $\{Cu_3(\mu\text{-}Cl)_2\}^{4+}$ subunit through the N1 and N2 positions and also to coordinate with the square-pyramidal Cu^3 site from the adjacent subunits through the N4 donor, extending the Cu^{II}_3 subunits into an infinite 3D framework of **2** (Fig. 2b). Topologically, each $\{Cu_3(\mu\text{-}Cl)_2\}^{4+}$ subunit is surrounded by eight neighbors through eight μ_3-tz^- connectors, and can act as an eight-connected node. Instead, the μ_3-tz^- ligand in **2** links two separate trinuclear subunits, behaving as a ditopic connector. Therefore, the overall 3D architecture of **2** is an eight-connected topological structure analogous to **1** (Fig. 2b). Notably, helical chains are observed running along the *c*-direction within the 3D framework of **2** (Fig. S2), which is constructed from Cu2 ions and the –NCN– moiety of asymmetric μ_3-tz^- ligand. The helical chain in **2** can induce an asymmetric magnetic exchange for potential canted antiferromagnetic behavior.[39]

$[Cu(N_3)(tz)]_n$ (3). Complex **3** is a square grid-like framework constructed from slightly bent

$\{Cu(\mu_{1,1}\text{-}N_3)\}^+$ chains and μ_3-N1, N2, N4-tz^- connectors. The asymmetric unit of **3** contains one Cu^{II} ion, one bridging azido anion and one anionic μ_3-tz^- ligand. The unique Cu^{II} ion in **3** assumes slightly distorted square-pyramidal N_5 coordination environment (τ = 0.004) completed by three tetrazolyl and two azido ligands (Fig. 3a and Table S3).

/insert Fig. 3/

Adjacent Cu^{II} ions of **3** are bridged by mixed $\mu_{1,1}$-N_3^- and tz^- bridges (Fig. 3b), leading to a slightly bent chain running along the crystallographic *a*-axis with the intermetallic separation and the angle of three neighboring Cu^{II} ions of 3.3934(3) Å and 165.299 (1)°. Notably, the azido bridge is in an end-on (EO) bridging mode ($\mu_{1,1}$-N_3^-) with ∠Cu–N–Cu = 116.45(2)°, favorable for antiferromagnetic interactions.[2] In addition to presenting two consecutive N donors to propagate the spin carriers into a 1D chain, the tz^- anion in **3** can further provide its N4 atom to bind with the metal ion from the adjacent chain, assembling the separate chains into a square grid-like 3D framework (Fig. 3c). The nearest interchain $Cu^{II}\cdots Cu^{II}$ distance (5.9514(5) Å) is almost twice the intrachain one favorable for weak interchain magnetic transfer.

$\{[Cu_5(tz)_9]Cl\cdot 4H_2O\}_n$ (4). Complex **4** without any co-coordinated inorganic anion/coligand crystallizes in the trigonal $P\bar{3}1c$ space group, displaying a hexagonal porous framework with trigonal prism-shaped $\{Cu_8(\mu_3\text{-}tz^-)_6\}^{10+}$ subunit interconnected by mirror-symmetry μ_4-tz^- ligands. The asymmetric unit of **4** consists of two Cu^{II} octahedra respectively located at inversion center (for Cu1) and passing through a 3-fold rotation axis (for Cu2), one and a half tz^- anions with asymmetric μ_3-N1,N2,N3- and mirror-symmetric μ_4-N1,N2,N3,N4-binding modes, 1/6 lattice chloride anion for charge compensation and some disordered free water molecules. The both Cu^{II} ions in **4** are surrounded by six N donors from six different tz^- ligands, exhibiting axially compressed and approximately ideal octahedra, respectively (Fig. 4a and Table S4).

/insert Fig. 4/

One Cu2 connects with three symmetry-related Cu1 octahedra through three μ_3-N1, N2, N3-tz$^-$ ligand, generating a flattened tetrahedral $\{Cu_4(\mu_3\text{-tz})_3\}^{5+}$ subunit with the apical Cu2 atom passing through a three-fold rotation axis (Fig. 4b). The intermetallic separations within the tetrahedral subunit are 6.1638(1) and 3.7698(1) Å for Cu1···Cu1 and Cu1···Cu2. Furthermore, pairs of $\{Cu_4(\mu_3\text{-tz})_3\}^{5+}$ subunits are periodically extended by three crystallographically equivalent μ_4-N1,N2,N3,N4-tz$^-$ ligands in an alternating head-to-head and tail-to-tail manner, leading to an infinite trigonal prism subunit running along the crystallographic *c* axis (Fig. 4b). Notably, the trigonal prism subunit of **4** contains a crystallographic C_3 rotation axis passing through the adjacent Cu2 ions and a mirror perpendicular to the molecular plane of μ_4-N1,N2,N3,N4-tz$^-$ connector.

As shown in Fig. 4c, each isolated trigonal prism of **4** connects with three neighbors through mirror-symmetric μ_4-N1,N2,N3,N4-tz$^-$ connector coordinating with the Cu2 ions from the adjacent subunit. As a result, a 3D porous framework with hexagonal channels is generated, in which the effective volume for the inclusion occupies 27.1% of the crystal volume calculated by PLATON software.[40]

Structural analyses of **1**–**4** indicate that the direct binding of tz$^-$ with Cu^{II} ion can result in a high-symmetrically porous framework. The involvement of the third component (SO_4^{2-}, Cl^- and N_3^-) destroys the skeletal symmetry and induces new subunits (hourglass-shaped $\{Cu_5(\mu_3\text{-OH})_2\}^{8+}$, linear $\{Cu_3(\mu\text{-Cl})_2\}^{4+}$ core and linear $\{Cu(\mu_{1,1}\text{-N}_3)\}^+$ chain) through the different coordination ability, bridging modes and steric hindrances. Moreover, the presence of the inorganic anion/coligand in the resulting complexes can further affect the binding manner of the tz$^-$ ligand, which corporately contributes to structural diversities of **1**–**4**.

Magnetic properties

Variable-temperature direct current (dc) magnetic susceptibilities were measured on the freshly prepared, crystalline samples of **1**–**4** under an applied field of 1 kOe. As shown in Fig. 5a, the $\chi_M T$ product per Cu^{II}_5 subunit of **1** is 1.87 cm^3 K mol^{-1} at 300 K, which is in good agreement with the spin-only value (1.87 cm^3 K mol^{-1}) expected for five magnetically isolated Cu^{II} ions with $S = 1/2$ and $g = 2.0$. Upon cooling, the $\chi_M T$ product slowly decreases to a local minimum at 16.0 K (0.67 cm^3 K mol^{-1}), indicating the antiferromagnetic interaction occurs through the μ_4-SO_4^{2-}, μ_3-OH^- and μ_4-tz^- heterobridges. Then, it rises rapidly to a sharp maximum of 11.78 cm^3 K mol^{-1} at 6.0 K, and finally drops to 4.83 cm^3 K mol^{-1} at 2.0 K due to the saturation effect and/or intercluster antiferromagnetic interactions. The abrupt increase of $\chi_M T$ at low temperature suggests an onset of a spontaneous magnetization due to the ferrimagnetic or canted antiferromagnetic interactions.

Field-dependent magnetization of **1** performed at 2.0 K (Fig. 5b) shows an initially rapid increase below 20 kOe and then slowly reaches the maximum value of 1.01 $N\mu_B$ at 70 kOe. The saturated magnetization at 70 kOe for each Cu^{II}_5 subunit of **1** is in good agreement with the theoretical value (1.00 $N\mu_B$) for one uncompensated Cu^{II} ion, meaning that a $S = 1/2$ spin ground-state is generated in each Cu^{II}_5 cluster (Fig. 5a, inset). Notably, the isothermal magnetization of **1** does not follow a Brillouin curve, confirming the classical ferrimagnetic behaviour of **1**. A magnetic hysteresis loop is observed at 2.0 K with a coercive field of 0.3 kOe and a remnant magnetization of 0.4 $N\mu_B$ for each Cu^{II}_5 subunit (Fig. 5b insert).

/insert Fig. 5/

Alternate current (ac) magnetic susceptibilities of **1** were measured under a zero dc field with an oscillating field of 3.5 Oe at frequencies of 10, 100 and 1000 Hz (Fig. 5c). Both in-phase (χ') and out-of-phase (χ'') ac signals are field-independent and exhibit a sharp peak at 7.0 K, indicating long-range ferromagnetic ordering of **1**. The Néel temperature (T_N) obtained from the ac susceptibilities is 7.0 K,

which is further confirmed by a clear bifurcation of the field-cooled (FC) and zero-field-cooled (ZFC) curves at *ca* 7.0 K (Fig. 5c inset). The magnetic ordering of **1** is significantly due to the distorted corner-sharing triangles with nonequivalent $Cu^{II}\cdots Cu^{II}$ separations and dihedral angles between μ_3-tz^-/μ_4-$tz^-$and Cu^{II}_5 plane (32.498º vs 5.296º) (Fig. S3).[41] Thus, the above magnetic results suggest that complex **1** is a 3D ferrimagnet. To the best of our knowledge, **1** is the first ferrimagnet among all the known Cu^{II}-tetrazolate-based magnetic systems, which is much different from the previously reported samples $[Cu_3(L)_2(VO_3)_4]_n$ (L = 5-(pyrimidin-2-yl)tetrazole) and $[Cu_5(tz)_6(CN)_2]_n$ modified by heterospins and mixed-valence copper(I, II) ions.[21, 42]

The $\chi_M T$ value per Cu^{II}_3 subunit of **2** at 300 K (0.90 cm^3 K mol^{-1}, Fig. 6a) is moderately lower than the spin-only value expected for three magnetically isolated Cu^{II} ions with S = 1/2 and g = 2.0 (1.12 cm^3 K mol^{-1}). The $\chi_M T$ product decreases continuously with the lowering temperature and is down to the minimum of 0.10 cm^3 K mol^{-1} at 14.0 K. Then, it increases rapidly to a sharp maximum of 0.80 cm^3 K mol^{-1} at 10.0 K, and finally drops probably due to the intercluster antiferromagnetic couplings. The increase of $\chi_M T$ observed at low temperature suggests a weak spontaneous magnetization by ferrimagnetism or canted antiferromagnetism. Moreover, the χ_M curves of **2** are field-dependent at low temperature (Fig. 6a inset).

The superexchange coupling of **2** is essentially dominated in the linear Cu^{II}_3 subunit, because the ternary heterobridges (one μ-Cl^- and double −NN− moieties of μ_3-tz^- ligands) can more effectively transfer the magnetic couplings than long −NCN− pathway of μ_3-tz^- bridges. Thus, the magnetic data of **2** can be fitted to a centrosymmetric linear trinuclear model with spin Hamiltonian operator $\boldsymbol{H} = -2J(\boldsymbol{S}_{Cu2}\boldsymbol{S}_{Cu1}+\boldsymbol{S}_{Cu1}\boldsymbol{S}_{Cu2A})$, in which the intercluster interaction term (zJ') by −NCN− of μ_3-tz^- bridge can be introduced by a molecular approximation.

$$\chi_{Cu_3^{II}} = \frac{Ng^2\beta^2}{4kT} \times \frac{1 + e^{-2J/kT} + 10e^{J/kT}}{1 + e^{-2J/kT} + 2e^{J/kT}} \quad (1)$$

$$\chi_M T = \frac{\chi_{Cu_3^{II}}}{1 - (2zJ'/Ng^2\beta^2)\chi_{Cu_3^{II}}} T \quad (2)$$

The least-squares fitting of magnetic susceptibilities of **2** to Eqs (1) and (2) above 14.0 K leads to g = 2.14, J_1 = –62.1 cm^{-1}, zJ' = –22.0 cm^{-1}, and R = 6.4 $\times 10^{-4}$, in which R is the agreement factor defined as $R = \Sigma[(\chi_M T)_{obsd} - (\chi_M T)_{calcd}]^2/\Sigma[(\chi_M T)_{obsd}]^2$. The obtained coupling constants indicate that the intercluster magnetic interactions are almost one third of the intracluster one, although they are comparable with those previously reported Cu^{II}-containing entities with analogous ternary heterobridges.[26, 43]

/insert Fig. 6/

The isothermal magnetization of **2** shows an abrupt increase below 0.1 kOe and is followed by a steady increase to 0.11$N\mu_B$ at 70 kOe, without achieving saturation even for one Cu^{II} ion (Fig. 6b). These resulting magnetic results jointly suggest **2** is a canted antiferromagnet induced by the asymmetric magnetic exchange in the –Cu2–NCN–Cu2 chain.[39] A hysteresis loop is observed at 2.0 K with a coercive field and the remnant magnetization of *ca.* 20 Oe and 0.01 $N\mu_B$ (Fig. 6b inset), being characteristic of a soft magnet. The canting angle (φ) is calculated to be ca. 0.25º based on $\varphi = \tan^{-1}(Mr/Ms)$.[44] The T_N value is verified by the ZFC and FC experiments with a divergence point at *ca*. 12.0 K (Fig. 6c inset) and the poignant peaks of real and imaginary ac components at 12.4 K (Fig. 6c).

Different from the former two samples with weak spontaneous magnetizations, **3** and **4** show typically antiferromagnetic interactions. The observed $\chi_M T$ values for **3** and **4** at 300 K (0.349 and 0.330 cm^3 K mol^{-1}, Fig. 7a) are slightly lower than the expected spin-only value (0.375 cm^3 K mol^{-1}) for one magnetically uncoupled Cu^{II} ion with S = 1/2 and g = 2.0. Upon cooling, the $\chi_M T$ products monotonously decrease in almost similar slopes and reach 0.005 (for **3**) and 0.015 cm^3 K mol^{-1} (for **4**) at 2.0 K, revealing that the antiferromagnetic interactions between the spin carriers lead to an overall S = 0 spin ground-state. Such

magnetic behavior can be further confirmed by the nearly zero magnetizations even at 70 kOe (0.08 and 0.07 $N\mu_B$ for **3** and **4**, Fig. 7b). A 1D chain model with the spin Hamiltonian $H = -J\sum_{i=1}^{n-1} S_{A_i} S_{A_{i+1}}$ is used to quantitatively describe the coupling strength by the binary heterobridges ($\mu_{1,1}$-N_3^- and –NN– of μ_3-tz^-) of **3**, in which the interchain magnetic interactions (zJ') mediated by –NNN–/–NCN– of μ_3-tz^- is taken into account by a molecular field approximation. The least-squares fitting of the magnetic data above 50 K to Eqs. (3) and (4) leads to $g = 2.17$, $J = -87.3$ cm^{-1}, $zJ' = -21.1$ cm^{-1} with $R = 6.2\times10^{-3}$.

$$\chi_{\text{chain}} = \frac{Ng^2\beta^2}{kT} \times \frac{0.25 + 0.074975x + 0.075235x^2}{1.0 + 0.9931x + 0.172135x^2 + 0.757825x^3} \qquad (3)$$

with $x = |J|/kT$

$$\chi_M T = \frac{\chi_{\text{chain}}}{1 - (2zJ'/Ng^2\beta^2)\chi_{\text{chain}}} \qquad (4)$$

Obviously, the intrachain antiferromagnetic interaction of **3** mediated by the double heterobridges is much stronger than those of **2** mediated by ternary ones (one μ-Cl^- and double $^-$NN$^-$ moieties of μ_3-tz^- ligands). The dihedral angles between the basal plane of adjacent spin carriers (28.547º for **2** and 80.658º for **3**) is also responsible for the coupling strength, in which the smaller angle can produce a relatively good magnetic overlap to give strong antiferromagnetic coupling.

/insert Fig. 7/

It is interesting to structurally and magnetically compare **3** with its analogue $[Cu(trz)(N_3)]_n$ with canted antiferromagnetism.[45] The two samples share the same composition, approximate crystal structures, and different magnetic behaviours. However, the spatial orientations of bridging azido group towards the Cu^{II} ions are different, which vitally directs the resulting magnetic properties. The bridging azido group in the $[Cu(trz)(N_3)]_n$ locates respectively at the basal and apical positions of the adjacent Cu^{II} ions, which produces a large bridging angels (117.4(1)^o) and an asymmetric magnetic exchange for the canted

antiferromagnetic behavior. While the azido group in **3** adopts a basal-basal connection with a slightly smaller bridging angle (116.45(2)°) than that of $[Cu(trz)(N_3)]_n$, and only results in the antiferromagnetic interactions of **3**.

Due to high and perfect symmetry of the magnetic framework, it is currently difficult to extract a suitable magnetic model to fit the magnetic susceptibilities of **4**. However, as compared with **2**, the absence of the co-coordinated Cl^- anion in the inner-sphere of **4** increases the symmetry of the overall framework, accompanying the appearance of a characteristic C_3 axis. The increased framework symmetry offsets the unsaturated magnetic moment from the spin carriers, resulting in simple antiferromagnetic couplings of **4**.

Conclusion

Four unsubstituted tetrazolate-based MMOFs were solvo/hydrothermally generated by the co-coordination of the small inorganic anions and/or the coligand. Crystallographically, the co-coordination of these accessorial species results in hourglass-shaped pentanuclear cluster, linear trinuclear subunit, linear chain, and trigonal prism block, which are further extended into four interesting 3D frameworks by multisite tetrazolate connectors. Antiferromagnetic couplings in the local subunits lead to non-zero and/or zero net magnetizations, which are arranged in the 3D frameworks by different linkers to result in the overall homospin ferrimagnet, canted antiferromagnet, as well as overall $S = 0$ spin ground-states.

Acknowledgements

The present work was financially supported by the National Natural Science Foundation of China (Grants 21171129, 21173157 and 21371134), the 973 Program (2014CB845601), the Program for Innovative Research Team in University of Tianjin (TD12−5038) and Tianjin Municipal Education Commission (2012ZD02), which are gratefully acknowledged.

References

1 M. Kurmoo, *Chem. Soc. Rev.*, 2009, **38**, 1353.
2 Y. F. Zeng, X. Hu, F. C. Liu and X. H. Bu, *Chem. Soc. Rev.*, 2009, **38**, 469.

3 J. H. Song, K. S. Lim, D. W. Ryu, S. W. Yoon, B. J. Suh and C. S. Hong, *Inorg. Chem.*, 2014, **53**, 7936.

4 S. Ganguly, P. Pachfule, S. Bala, A. Goswami, S. Bhattacharya and R. Mondal, *Inorg. Chem.*, 2013, **52**, 3588.

5 S. T. Zheng, T. Wu, J. Zhang, M. Chow, R. A. Nieto, P. Y. Feng and X. H. Bu, *Angew. Chem., Int. Ed.*, 2010, **49**, 5362.

6 Y. Q. Wang, Q. Yue, Y. Qi, K. Wang, Q. Sun and E. Q. Gao, *Inorg. Chem.*, 2013, **52**, 4259.

7 L. N. Jia, L. Hou, L. Wei, X. J. Jing, B. Liu, Y. Y. Wang and Q. Z. Shi, *Cryst. Growth Des.*, 2013, **13**, 1570.

8 (a) E. C. Yang, Z. Y. Liu, X. Y. Wu and X. J. Zhao, *Chem. Commun.*, 2011, **47**, 8629; (b) E. C. Yang, Y. Y. Zhang, Z. Y. Liu and X. J. Zhao, *Inorg. Chem.*, 2014, **53**, 327.

9 W. Ouellette, S. Jones and J. Zubieta, *CrystEngComm*, 2011, **13**, 4457.

10 S. H. Wang, F. K. Zheng, M. J. Zhang, Z. F. Liu, J. Chen, Y. Xiao, A. Q. Wu, G. C. Guo and J. S. Huang, *Inorg. Chem.*, 2013, **52**, 10096.

11 J. P. Zhang, Y. B. Zhang, J. B. Lin and X. M. Chen, *Chem. Rev.*, 2012, **112**, 1001.

12 Z. Yan, M. Li, H. L. Gao, X. C. Huang and D. Li, *Chem. Commun.*, 2012, **48**, 3960.

13 T. W. Tseng, T. T. Luo, S. Y. Chen, C. C. Su, K. M. Chi and K. L. Lu, *Cryst. Growth Des.*, 2013, **13**, 510.

14 X. B. Li, G. M. Zhuang, X. Wang, K. Wang and E. Q. Gao, *Chem. Commun.*, 2013, **49**, 1814.

15 (a) H. Park, J. F. Britten, U. Mueller, J. Y. Lee, J. Li and J. B. Parise, *Chem. Mater.*, 2007, **19**, 1302; (b) H. Park, D. M. Moureau and J. B. Parise, *Chem. Mater.*, 2006, **18**, 525.

16 (a) C. P. Ma, Y. G. Li, H. H. Zhao, B. Li, J. R. Cheng, P. Balbuena and H. C. Zhou, *J. Am. Chem. Soc.*, 2012, **134**, 18892; (b) M. Wriedt, A. A. Yakovenko, G. J. Halder, A. V. Prosvirin, K. R. Dunbar and H. C. Zhou, *J. Am. Chem. Soc.*, 2013, **135**, 4040.

17 A. Rodríguez Diéguez, M. A. Palacios, A. Sironib and E. Colacio, *Dalton Trans.*, 2008, 2887.

18 X. He, C. D. Wu, M. X. Li and S. R. Batten, *Inorg. Chem. Commun.*, 2008, **11**, 1378.

19 L. Carlucci, G. Ciani and D. M. Proserpio, *Angew. Chem., Int. Ed.*, 1999, **38**, 3488.

20 X. M. Zhang, J. Lv, F. Ji, H. S. Wu, H. J. Jiao and P. v. R. Schleyer, *J. Am. Chem. Soc.*, 2011, **133**, 4788.

21 X. M. Zhang, Y. F. Zhao, X. W. Zhang and X. M. Chen, *Adv. Mater.*, 2007, **19**, 2843.

22 Z. P. Deng, Z. B. Zhu, X. F. Zhang, L. H. Huo, H. Zhao and S. Gao, *CrystEngComm*, 2011, **13**, 3895.

23 Y. C. Chuang, C. T. Liu, C. F. Sheu, W. L. Ho, G. H. Lee, C. C. Wang and Y. Wang, *Inorg. Chem.*, 2012, **51**, 4663.

24 X. H. Jin, J. K. Sun, L. X. Cai and J. Zhang, *Chem. Commun.*, 2011, **47**, 2667.

25 H. Lee, S. H. Jung, W. S. Han, J. H. Moon, S. Kang, J. Y. Lee, J. H. Jung and S. Shinkai, *Chem.–Eur. J.*, 2011, **17**, 2823.

26 W. Ouellette, A. V. Prosvirin, V. Chieffo, K. R. Dunbar, B. Hudson and J. Zubieta, *Inorg. Chem.*, 2006, **45**, 9346.

27 D. Zhang, Y. Lu, D. Zhu and Y. Xu, *Inorg. Chem*., 2013, **52**, 3253.

28 R. J. Goetz, A. Robertazzi, I. Mutikainen, U. Turpeinen, P. Gamez and J. Reedijk, *Chem. Commun.*, 2008, 3384.

29 D. L. Long, R. J. Hill, A. J. Blake, N. R. Champness, P. Hubberstey, C. Wilson and M. Schroeder, *Chem.–Eur. J.*, 2005, **11**, 1384.

30 J. Y. Liu, Q. Wang, L. J. Zhang, B. Yuan, Y. Y. Xu, X. Zhang, C. Y. Zhao, D. Wang, Y. Yuan, Y. Wang,

B. Ding, X. J. Zhao and M. M. Yue, *Inorg. Chem*., 2014, **53**, 597.
31 S. Hou, Q. K. Liu, J. P. Ma and Y. B. Dong, *Inorg. Chem*., 2013, **52**, 3225.
32 T. Liu, Y. H. Chen, Y. J. Zhang, Z. M. Wang and S. Gao, *Inorg. Chem.*, 2006, **45**, 9148.
33 Z. Y. Liu, Y. H. Su, E. C. Yang and X. J. Zhao, *Inorg. Chem. Commun*., 2012, **26**, 56.
34 G. M. Sheldrick, *SADABS*, University of Göttingen, Göttingen, Germany, 1996.
35 Bruker AXS, *SAINT software Reference Manual*, Madison, WI, 1998.
36 (a) G. M. Sheldrick, *SHELXL-97, Program for X-ray Crystal Structure Refinement*; Göttingen University: Göttingen, Germany, 1997; (b) G. M. Sheldrick, *SHELXS-97, Program for X-ray Crystal Structure Solution*; Göttingen University: Göttingen, Germany, 1997.
37 K. Nakamoto, *Infrared and Roman Spectra of Inorganic and Coordination Compounds*, Wiley, New York, 1986.
38 A. W. Addison, T. N. Rao, J. Reedijk, J. v. Rijn and G. C. Verschoor, *J. Chem. Soc. Dalton Trans*., 1984, 1349.
39 (a) R. L. Carlin, *Magnetochemistry*, Springer-Verlag, Berlin, 1986; (b) O. Kahn, *Molecular Magnetism*, VCH, Weinheim, 1993.
40 P. van der Sluis and A. L. Spek, *Acta Crystallogr.*, *Sect. A*. 1990, **46**, 194.
41 (a) Y. Zhao, M. Padmanabhan, Q. Gong, N. Tsumori, Q. Xu and J. Li, *Chem. Commun*., 2011, **47**, 6377; (b) R. Nath, A. A. Tsirlin, P. Khuntia, O. Janson, T. Förster, M. Padmanabhan, J. Li, Y. SKourski, M. Baenitz, H. Rosner and I. Rousochatzakis, *Phys. Rev. B*., 2013, **87**, 214417.
42 J. R. Li, Q. Yu, E. C. Sañudo, Y. Tao, W. C. Song and X. H. Bu, *Chem. Mater*., 2008, **20**, 1218.
43 Z. Y. Liu, H. A. Zou, Z. J. Hou, E. C. Yang and X. J. Zhao, *Dalton Trans*., 2013, **42**, 15716.
44 F. Palacio, M. Andres, R. Horne and A. J. Van Duynevelt, *J. Magn. Magn. Mater*., 1986, **54-57**, 1487.
45 J. R. Li, Q. Yu, E. C. Sañudo, Y. Tao and X. H. Bu, *Chem. Commun*., 2007, 2602.

Table 1 Crystal data and structure refinement for **1**–**4** [a]

	1	**2**	**3**	**4**
Chemical formula	$C_8H_{12}Cu_{10}N_{32}O_{20}S_4$	$C_{5.40}H_{9.60}Cl_2Cu_3N_{16}O_{1.40}$	$CHCuN_7$	$C_3H_{5.67}Cl_{0.33}Cu_{1.67}N_{12}O_{1.33}$
f_w	1640.14	582.61	174.63	348.91
crystal size /mm	0.18 × 0.17 × 0.16	0.10 × 0.08 × 0.07	0.15 × 0.05 × 0.04	0.18 × 0.17 × 0.15
Temperature	173	296	173	296
Crystal sys	monoclinic	orthorhombic	orthorhombic	trigonal
space group	$P2_1/n$	$Pnnm$	$P2_12_12_1$	$P\bar{3}1c$
a /Å	8.6031(5)	11.6119(6)	6.7311(7)	12.3275(3)
b /Å	8.5338(5)	8.6116(5)	7.4805(10)	12.3275(3)
c /Å	13.3805(8)	8.8761(5)	9.6521(10)	12.5415(7)
β /°	106.7950(10)	90.00	90.00	90.00
γ /°	90.00	90.00	90.00	120.00
V /Å^3	940.46(10)	887.58(9)	486.00(10)	1650.55(11)
Z	1	2	4	6
h / k / l	– 7, 10 / – 10, 9 / – 15, 15	– 12,13 / – 10,10 / – 10,8	– 7, 9 / – 9, 10 / – 12, 9	– 14, 9 / – 10, 14 / – 14, 14
F(000)	798	572	340	1026
reflections collected / unique	5277 / 1655	4861 / 842	3688 / 1229	8985 / 956
R_{int}	0.0312	0.0228	0.0363	0.0458
data / restraints / params	1655 / 30 / 169	842 / 14 / 76	1229 / 48 / 83	956 / 45 / 99
R_1 [a], wR_2 [b] [$I > 2\sigma$ (I)]	0.0228 / 0.0515	0.0342 / 0.0982	0.0263 / 0.0571	0.0575 / 0.1247
R_1, wR_2 [all data]	0.0263 / 0.0532	0.0369 / 0.1026	0.0289 / 0.0580	0.0651 / 0.1290
Max. and min. transmission	0.4530 / 0.4175	0.7718 / 0.6962	0.8441 / 0.5591	0.6346 / 0.5851
GOF on F^2	1.018	1.211	1.066	1.166
$\Delta\rho_{max}$, $\Delta\rho_{min}$ / e·Å^{-3}	0.465 / – 0.490	2.079 / – 0.609	0.873 / – 0.514	0.545 / – 0.616

[a] $R_1 = \Sigma(||F_o|-|F_c||)/\Sigma|F_o|$. [b] $wR_2 = [\Sigma w(|F_o|^2-|F_c|^2)^2/\Sigma w(F_o^2)^2]^{1/2}$.

Captions to Figures

Fig. 1 (a) Local coordination environments of Cu^{II} atoms in the pentanuclear cluster of **1**. H atoms were omitted for clarity, symmetry codes: A = 1 – *x*, – *y*, 1 – *z*; B = *x* – 1, *y*, *z*; C = 1/2 – *x*, *y* – 1/2, 3/2 – *z*; D = 1 – *x*, 1 – *y*, 1 – *z*. Selected bond lengths (Å): Cu1–O3 2.252(2), Cu1–O5 2.056(2), Cu1–N6 1.991(3), Cu2–O5 2.004(2), Cu2–O1 1.968(2), Cu2–N7 2.414(3), Cu3–O2 2.256(2). (b) Linkages of the $\{Cu_5(\mu_3\text{-}OH)_2\}^{8+}$ core with mixed μ_4-SO_4^{2-} and μ_3-/μ_4-tz^- connectors. (c) 3D framework of **1** and its topological representation.

Fig. 2 (a) Local coordination environments of Cu^{II} atoms in **2**. H atoms were omitted for clarity, symmetry codes: A = *x*, *y*, 1 – *z*; B = 1 – *x* , 1 – *y*, *z*; C = 1 – *x*, 1 – *y*, 1 – *z*; D = 3/2 – *x*, *y* + 1/2, 1/2 – *z*; E = 3/2 – *x*, *y* + 1/2, *z* + 1/2. Selected bond lengths (Å): Cu1–N2 2.022(3), Cu1–Cl1 2.6050(16), Cu2–N1 2.056(4), Cu2–N4 2.009(4), Cu2–Cl1 2.4743(16). (b) Linkages of Cu^{II}_3 subunit with μ_3-tz^- ligand and the 8-connected topological representation of **2**.

Fig. 3 (a) Local coordination environments of Cu^{II} atoms in **3**. H atoms were omitted for clarity, symmetry codes: A = 0.5 – *x*, 1 – *y*, *z* – 1/2; B = – *x*, 1/2 + *y*, 1/2 – *z*; C = *x* – 1/2, 3/2 – *y*, – *z*. Selected bond lengths (Å): Cu1–N1 2.204(3), Cu1–N5 1.991(3), Cu1–N5C 2.000(2), Cu1–N3 1.986(3), Cu1–N4A 1.981(3). (b) 1D bent chain of **3** linked by mixed tz^- and azido heterobridges. (c) 3D grid-like framework of **3** constructed from 1D chains and ditopic μ_3-tz^- connectors.

Fig. 4 (a) Local coordination environments of Cu^{II} atoms in **4**. H atoms were omitted for clarity, symmetry codes: A = *x* – *y*, *x*, 2 – *z*; B = 1– *x* + *y*, 1 – *x*, *z*; C = 1 – *x*, 1 – *y*, 2 – *z*; D = 1 – *y*, *x* – *y*, *z*; E = 1 – *y*, 1 – *x*, 1.5 – *z*. Selected bond lengths (Å): Cu1–N5 2.100(7), Cu1–N7 2.134(6), Cu1–N3 2.142(6), Cu2–N4 2.120(6), Cu2–N6 2.096(7). (b) Trigonal prism substructure in **4**. (c) 3D framework of **4** constructed from the connections of trigonal prism substructure.

Fig. 5 (a) Temperature dependency of $\chi_M T$ for **1** (Inset: magnetic interactions in the Cu^{II}_5 cluster). (b) Field-dependent magnetization of **1** measured at 2.0 K (Inset: magnetic hysteresis loop for **1** at 2.0 K). (c) Temperature dependence of the ac susceptibilities for **1** at different frequencies under H_{ac}= 3.5 Oe and H_{dc} = 0 Oe (Inset: FC and ZFC magnetizations).

Fig. 6 (a) Temperature dependency of $\chi_M T$ for **2** (Inset: temperature dependence of χ_M at various dc fields). (b) Field-dependent magnetization of **2** measured at 2.0 K (Inset: magnetic hysteresis loop for **2** at 2.0 K). (c) Temperature dependence of the ac susceptibilities for **2** at different frequencies under H_{ac}= 3.5 Oe and H_{dc}= 0 Oe (Inset: FC and ZFC magnetizations).

Fig. 7 (a) Temperature dependency of $\chi_M T$ for **3** and **4** (Solid line represents the best fit indicated in the text). (b) Field-dependent magnetizations of **3** and **4** measured at 2.0 K.

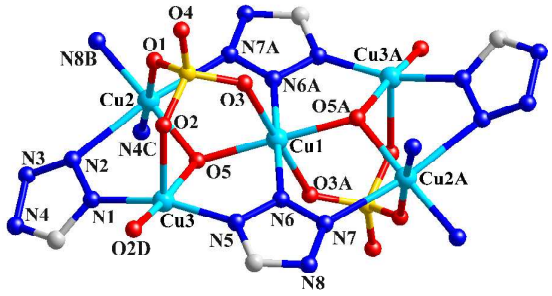

(a)

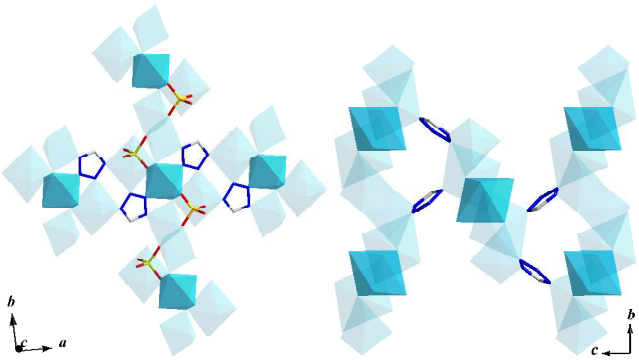

(b)

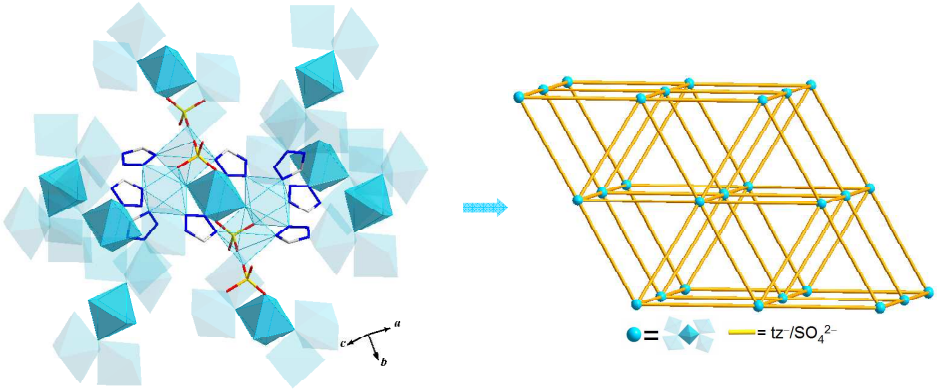

(c)

Fig. 1

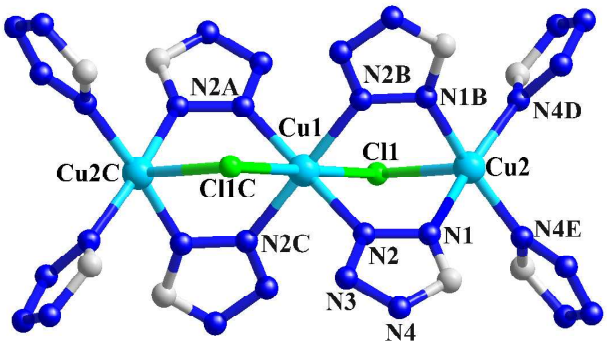

(a)

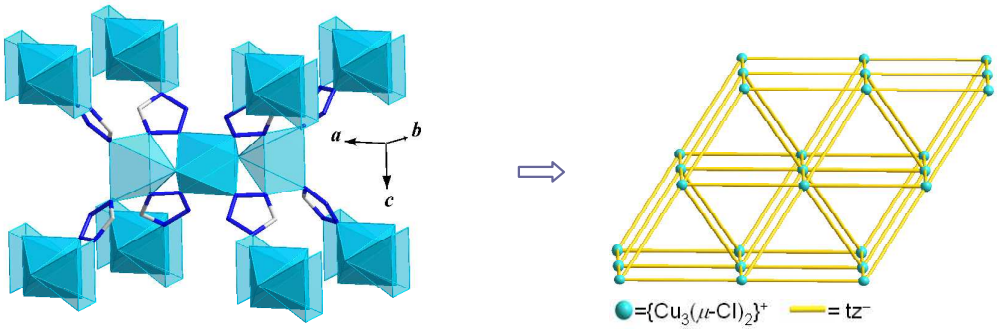

(b)

Fig. 2

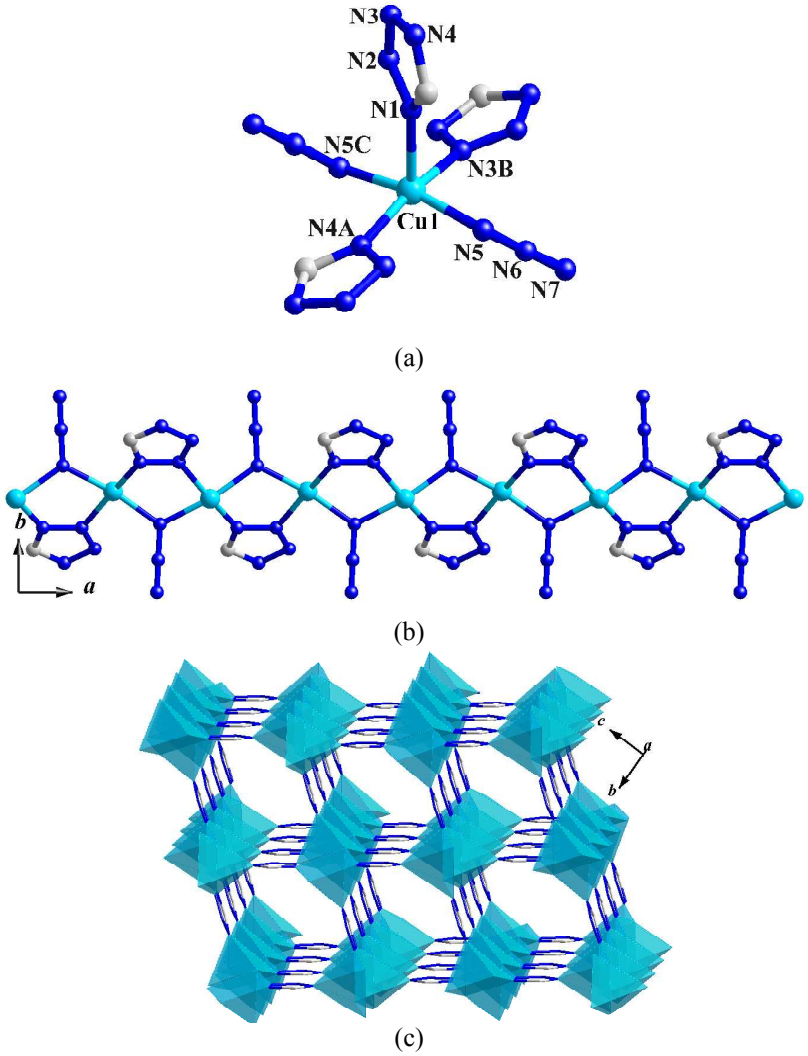

Fig. 3

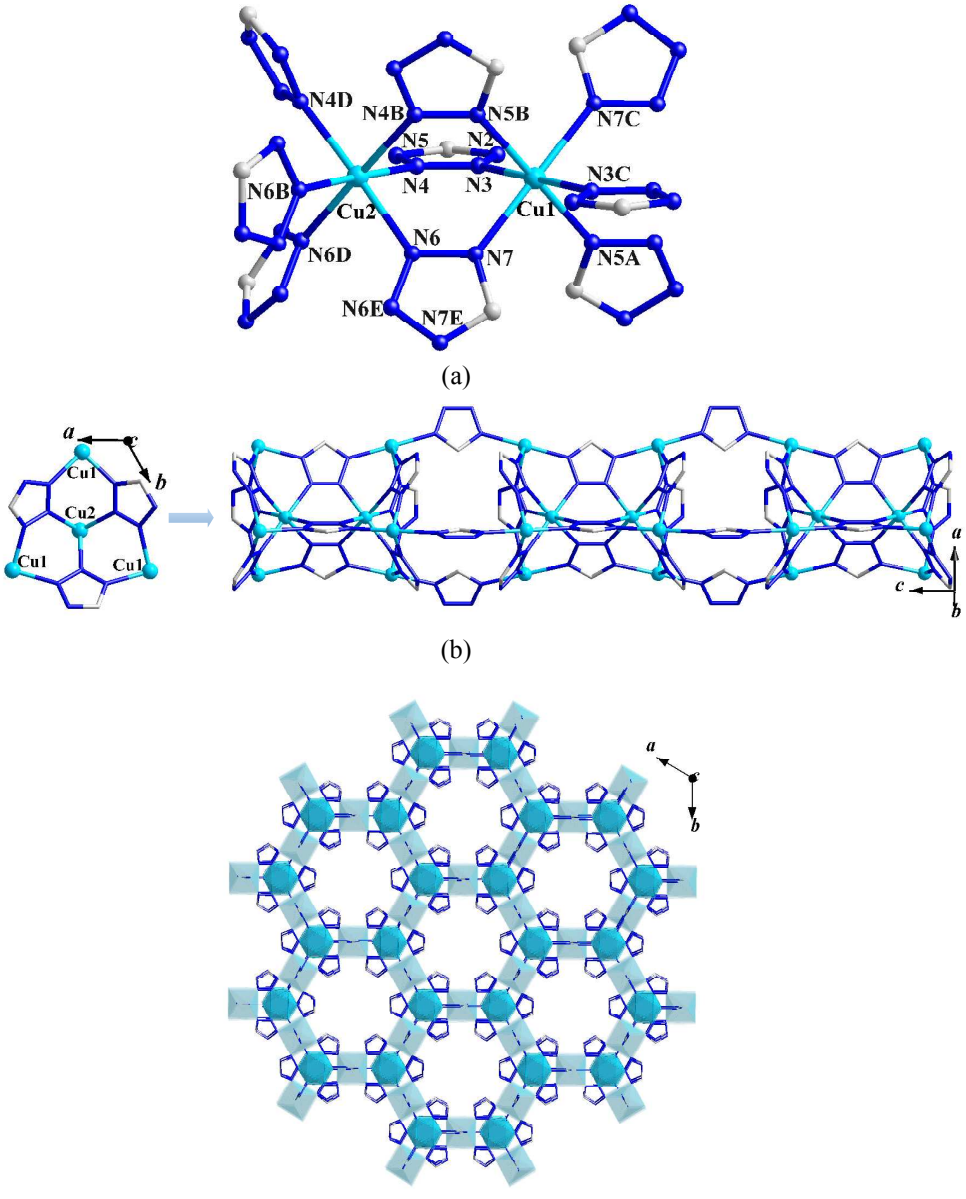

Fig. 4

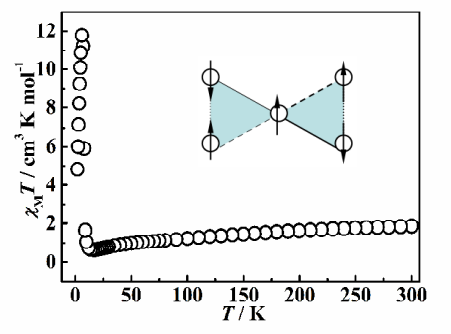

(a)

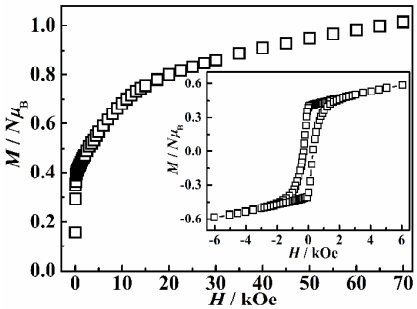

(b)

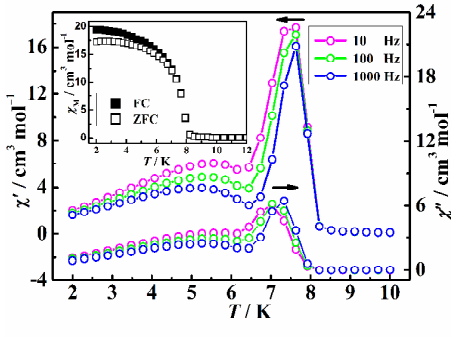

(c)

Fig. 5

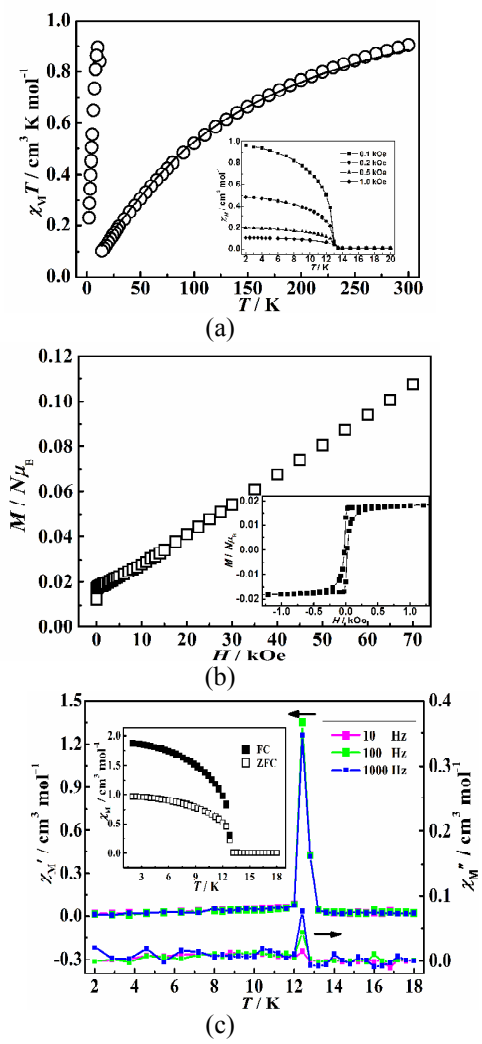

Fig. 6

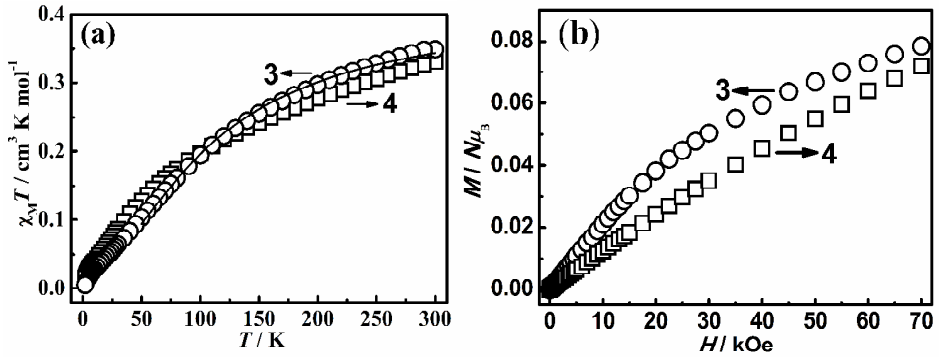

Fig. 7

Graphic abstract

Four tetrazolate-based 3d frameworks with diverse subunits directed by inorganic anions and azido coligand: hydrothermal syntheses, crystal structures, and magnetic properties

Zhao-Jun Hou,[a] Zhong-Yi Liu,[a] Ning Liu,[a] En-Cui Yang[a, *] and Xiao-Jun Zhao[a, b *]

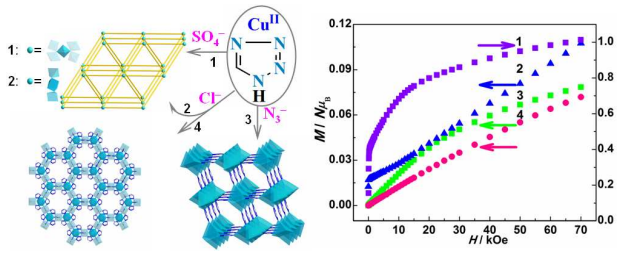

Co-coordination of the inorganic anions or azido coligand in the Cu^{II}-tetrazolate system results in hourglass-shaped $\{Cu_5(\mu_3\text{-}OH)_2\}^{8+}$ cluster, linear $\{Cu_3(\mu\text{-}Cl)_2\}^{4+}$ core, linear $\{Cu(\mu_{1,1}\text{-}N_3)\}^{+}$ chain and trigonal-prismatic $\{Cu_8(\mu_3\text{-}tz)_6\}^{10+}$ motifs, which are further extended into two eight-connected frameworks with ferrimagnetic and canted antiferromagnetic behaviors, one square grid-shaped network and one hexagonal microporous architecture with $S = 0$ spin ground-states.